ELSEVIER

Journal of Nuclear Materials 240 (1997) 131–143

journal of nuclear materials

Isothermal diffusion in uranium–plutonium–zirconium alloys [1]

M.C. Petri [a,*], M.A. Dayananda [b]

[a] Argonne National Laboratory, 9700 South Cass Avenue, Argonne, IL 60439, USA
[b] Purdue University, School of Materials Engineering, West Lafayette, IN 47907, USA

Received 4 April 1996; accepted 9 September 1996

Abstract

Isothermal diffusion couple experiments were performed at 1023 K to investigate diffusion phenomena in body-centered cubic U–Pu–Zr alloys. The U–Pu–Zr alloys covered the uranium-rich corner of the ternary phase diagram with plutonium concentrations up to 27 at.% and zirconium concentrations up to 20 at.%. Ternary interdiffusion coefficients were calculated at the common composition between two couples with intersecting diffusion paths. The cross interdiffusion coefficient for zirconium ($\tilde{D}^{U}_{ZrPu}$) is negative and has a magnitude twice that of the main coefficient ($\tilde{D}^{U}_{ZrZr}$). In contrast, $\tilde{D}^{U}_{PuZr}$ is negligible compared with $\tilde{D}^{U}_{PuPu}$. $\tilde{D}^{U}_{PuPu}$ is an order of magnitude greater than $\tilde{D}^{U}_{ZrZr}$. Average effective interdiffusion coefficients were determined for all components over concentration ranges on the two sides of the Matano plane as well as for the entire diffusion zone of the couples. In general, these coefficients increase with increasing plutonium concentration and decrease with increasing zirconium concentration.

1. Introduction

U–Pu–Zr ternary alloys have been considered for fuel in advanced American [1] and Japanese [2] nuclear reactor concepts. This application requires an understanding of diffusion in the alloy system. An experimental determination of diffusion coefficients from U–Pu–Zr diffusion couples, however, poses unique challenges because the U–Pu–Zr alloys are radioactive and highly oxidizing. Limited interdiffusion studies have been conducted using U–Zr and Pu–Zr binary alloys in the bcc phase [3–6], and thermodynamic information has been calculated for the U–Pu–Zr ternary system [7]. In this system, each component has a high-temperature bcc phase (γ-U, ϵ-Pu, and β-Zr) that exists up to the melting temperature. Self-diffusion in these phases is anomalous in that the diffusivities are high, the activation energies and frequency factors are low, and semi-logarithmic plots of diffusivity versus reciprocal temperature (Arrhenius plots) are curved [8–10]. No published diffusion data exist for the ternary body-centered cubic (bcc) phase [11].

In this study, interdiffusion and intrinsic diffusion are examined for the bcc phase of the ternary uranium–plutonium–zirconium system. Interdiffusion and intrinsic diffusion coefficients were determined at 1023 K with solid–solid diffusion couples assembled with U–Pu–Zr alloys. To overcome the experimental challenges, techniques were developed to remotely perform and analyze isothermal diffusion experiments within plutonium gloveboxes. The experimental ternary diffusion couples included ones with similar Zr, U, or Pu concentrations in the terminal alloys for an assessment of the kinetic interactions among the components. The ternary interdiffusion coefficients were determined from couples with intersecting diffusion paths as well as from couples exhibiting maxima and minima in the concentration profiles. The ternary intrinsic diffusion coefficients were determined at compositions of markers in the diffusion zones. Average effective interdiffusion coefficients and effective penetration depths

* Corresponding author. Tel.: +1-630 252 3719; fax: +1-630 252 4922; e-mail: mcpetri@anl.gov.

[1] The submitted manuscript has been authored by a contractor of the US Government under contract No. W-31-109-ENG-38. Accordingly, the US Government retains a non-exclusive, royalty-free license to publish or reproduce the published form of this contribution or allow others to do so, for US Government purposes.

PII S0022-3115(96)00669-1

for the components were also determined on either side of the Matano plane for the various couples.

2. Background

2.1. Interdiffusion

Concentration profiles for each component developed in a diffusion couple are determined by an analysis of the compositions at different locations along the diffusion zone. From the concentration profiles one seeks to evaluate interdiffusion coefficients and other fundamental diffusion parameters.

Dayananda and Kim [12] have shown that the interdiffusion flux $\tilde{J}_i$ can be determined at any position x along the diffusion zone:

$$\tilde{J}_i(x) = \frac{1}{2t}\left[C_i^-(x_o - x^-) + C_i(x)(x - x_o) - \int_{x^-}^{x} C_i(x)\,dx\right] \quad (i = 1, 2, \ldots, n). \tag{1}$$

Here, x^- is an arbitrary position beyond the left end of the diffusion zone, C_i^- is the terminal concentration of component i at the left end of the diffusion zone, and t is the annealing time. The Matano plane position, x_o, represents the original contact plane at which, at any time, the accumulation of a component on one side is balanced by a depletion on the other side of the plane. Provided that there are no substantial molar volume changes, the position of the Matano plane is unique to a diffusion couple and can be calculated independently for any component i.

From Fick's First Law for one-dimensional diffusion in a binary system, the interdiffusion flux is expressed by

$$\tilde{J}_i(x) = -\tilde{D}\left(\frac{\partial C_i}{\partial x}\right)_t \quad (i = 1, 2), \tag{2}$$

where the interdiffusion flux of either component is proportional to its own concentration gradient through a single interdiffusion coefficient $\tilde{D}$, which is generally a function of composition. Since the interdiffusion flux can be determined at any position within the diffusion zone of a diffusion couple (Eq. (1)), a single experiment can be used to determine the binary $\tilde{D}$ as a function of position and, thus, as a function of composition from Eq. (2).

Onsager [13,14] generalized Fick's First Law by relating the flux to a linear combination of independent concentration gradients. For a ternary system, the interdiffusion fluxes of components 1 and 2 are given by

$$\tilde{J}_1(x) = -\tilde{D}_{11}^3\left(\frac{\partial C_1}{\partial x}\right)_t - \tilde{D}_{12}^3\left(\frac{\partial C_2}{\partial x}\right)_t, \tag{3}$$

$$\tilde{J}_2(x) = -\tilde{D}_{21}^3\left(\frac{\partial C_1}{\partial x}\right)_t - \tilde{D}_{22}^3\left(\frac{\partial C_2}{\partial x}\right)_t. \tag{4}$$

To determine the four independent interdiffusion coefficients $\tilde{D}_{ij}^3$, two diffusion couples that develop a common composition in their diffusion zones are required. Only at the common composition can the four interdiffusion coefficients be calculated. If the concentration gradient of component 1 approaches zero at some position in the diffusion zone, $\tilde{D}_{22}^3$ and $\tilde{D}_{12}^3$ can be determined at that location from a single diffusion couple experiment—provided that $(\partial C_2/\partial x)$ is also not near zero [15].

For the $\tilde{D}_{ij}^3$ matrix, component 3 has been chosen as the solvent; i.e., as the dependent concentration variable. For a ternary system with constant molar volume, the $\tilde{D}_{ij}^3$ coefficients can be converted to $\tilde{D}_{ij}^2$ coefficients with component 2 as the solvent through the following relationships [15]:

$$\tilde{D}_{11}^2 = \tilde{D}_{11}^3 - \tilde{D}_{12}^3, \tag{5}$$

$$\tilde{D}_{13}^2 = -\tilde{D}_{12}^3, \tag{6}$$

$$\tilde{D}_{31}^2 = \tilde{D}_{22}^3 + \tilde{D}_{12}^3 - \tilde{D}_{11}^3 - \tilde{D}_{21}^3, \tag{7}$$

$$\tilde{D}_{33}^2 = \tilde{D}_{22}^3 + \tilde{D}_{12}^3. \tag{8}$$

Similar relationships hold for the $\tilde{D}_{ij}^1$ coefficients with component 1 as the solvent.

2.2. Average effective interdiffusion coefficients

As a simplification, Dayananda and Behnke [16] have proposed reducing the interdiffusion coefficient matrix to a single 'average effective interdiffusion coefficient' for each component. This coefficient relates a component's interdiffusion flux and its concentration gradient and can be expressed by

$$\tilde{D}_i^{\text{eff}} = \tilde{D}_{ii}^3 + \frac{\tilde{D}_{ij}^3\left(\partial C_j/\partial x\right)_t}{\left(\partial C_i/\partial x\right)_t} \quad (i, j = 1, 2; j \neq i) \tag{9}$$

on the basis of Eqs. (3) and (4). $\tilde{D}_i^{\text{eff}}$ includes the effect of the cross-diffusivity terms, yet a component's flux can be calculated directly from a single concentration gradient if $\tilde{D}_i^{\text{eff}}$ is known. The average effective interdiffusion coefficient for each component can be determined for any region between x_1 and x_2 in the diffusion zone from the following relation [16]:

$$\tilde{D}_{i_{(1)}(x_2)}^{\text{eff}} = \frac{\tilde{J}_{i_{(1)}}(x_1 - x_o) - \tilde{J}_{i_{(2)}}(x_2 - x_o)}{C_{i_{(2)}} - C_{i_{(1)}}} + \frac{(x_2 - x_o)^2 C_{i_{(2)}} - (x_1 - x_o)^2 C_{i_{(1)}}}{2t\left(C_{i_{(2)}} - C_{i_{(1)}}\right)} - \frac{\int_{x_1}^{x_2} C_i(x - x_o)\,dx}{t\left(C_{i_{(2)}} - C_{i_{(1)}}\right)}. \tag{10}$$

$\tilde{D}_i^{\text{eff}}$ has been calculated for the binary and ternary diffusion couples over the concentration ranges on either side of the Matano plane, x_o, as well as over the entire

diffusion zone. From such coefficients, one can calculate an effective penetration depth ($\bar{x}_i$) for a component i on a given side of the Matano plane from the relation

$$\bar{x}_i = \sqrt{2t\tilde{D}_i^{\text{eff}}}, \tag{11}$$

where $\tilde{D}_i^{\text{eff}}$ is the calculated average effective interdiffusion coefficient for that side. The penetration depth of a component is proportional to the square root of the annealing time.

2.3. Intrinsic diffusion

The interdiffusion flux $\tilde{J}_i$ (based on a laboratory-fixed frame of reference) refers to the transport of atoms past a fixed, external reference frame. In contrast, the *intrinsic* flux J_i is based on a lattice-fixed frame of reference. Although the interdiffusion fluxes of all components must sum to zero, inert markers placed at the original contact plane of a diffusion couple will migrate with time owing to a net flux of vacancies. That is, intrinsically the components diffuse at different rates; the net flow is balanced by a vacancy flux:

$$\sum_{i=1}^{n} J_i + J_v = 0. \tag{12}$$

Here, J_i is the intrinsic flux for the ith component and J_v is the vacancy flux. As the migrating vacancies are destroyed at sinks, the lattice planes and markers shift in the direction of the net vacancy flow (the Kirkendall shift).

Following a procedure first proposed by Heumann [17], the composition profile can be used to measure the total amount of a component that diffuses past a marker plane, which is identified as the cumulative intrinsic flux A_i. This quantity can be expressed by

$$A_i = C_i^{+}(x_o - x^{+}) + \int_{x_m}^{x^{+}} C_i \, dx \quad (i = 1, 2, \ldots, n), \tag{13}$$

where x_m is the marker plane position at time t. The cumulative intrinsic flux is defined as the intrinsic flux at the marker plane integrated over time [18]. That is,

$$A_i = \int_0^t (J_i)_{x_m} \, dt = 2t(J_i)_{x_m} \quad (i = 1, 2, \ldots, n). \tag{14}$$

Therefore, the intrinsic flux at the marker plane for each component can be determined from the cumulative intrinsic flux. The sum of all cumulative intrinsic fluxes is related to the distance from the marker plane (x_m) to the Matano plane (x_o) for a constant-density (ρ) system:

$$\sum_{i=1}^{n} \frac{A_i}{\rho} = x_o - x_m. \tag{15}$$

A generalized form of Fick's First Law relates the intrinsic fluxes to the $n-1$ independent concentration gradients by an $n \times (n-1)$ matrix of intrinsic diffusion coefficients, D_{ij}^n:

$$J_i(x) = -\sum_{j=1}^{n-1} D_{ij}^n \left(\frac{\partial C_j}{\partial x}\right)_t \quad (i = 1, 2, \ldots, n). \tag{16}$$

For a binary system,

$$A_1 = -2tD_1\left(\frac{\partial C_1}{\partial x}\right)_{t, x_m}, \qquad A_2 = -2tD_2\left(\frac{\partial C_2}{\partial x}\right)_{t, x_m}, \tag{17}$$

where D_1 and D_2 are the two intrinsic diffusion coefficients that can be determined at the marker plane from a single experiment. In higher-order systems, $n-1$ diffusion couples with identical marker plane compositions would be needed to determine the D_{ij}^n coefficients. This requirement is hard to realize for solid–solid couples, but may be achieved in vapor–solid couples [19].

3. Experimental procedure

Nine diffusion couple experiments were conducted with alloys selected from the uranium-rich corner of the U–Pu–Zr ternary phase diagram. The couples are listed in Table 1. Couples 1 and 2 had terminal alloys with similar uranium concentrations. Similarly, the couple 3 alloys had equivalent zirconium concentrations and the couple 6 alloys had equivalent plutonium concentrations. All couples were annealed at 1023 K in a high-purity helium atmosphere. At this temperature all alloys are in the bcc γ-U phase field, except for the pure uranium sample, which is in the tetragonal β-U phase region. Except for couple 9, which was annealed for 25 h [20], all couples were annealed for 16.5 h. The present description of alloy preparation and experiment procedures applies strictly to couples 1 through 8 and to the alloys other than U–27Pu.

All alloys were available as cast rods with diameters ranging from 4.3 mm to 7.3 mm. The bars were given a four-day 1093 K heat treatment in helium to promote grain growth and homogenization. Pieces cut from the annealed

Table 1
Diffusion couples annealed at 1023 K for 16.5 h

Couple	Diffusion couple alloys
1, 2 [a]	U–20Zr versus U–22Pu–3Zr [b]
3	U–20Zr versus U–22Pu–20Zr
4, 5 [a]	U versus U–22Pu–20Zr
6	U–22Pu–3Zr versus U–22Pu–20Zr
7	U versus U–22Pu–3Zr
8	U versus U–20Zr
9	U versus U–27Pu [c]

[a] Couples 1 and 2 and couples 4 and 5 are duplicate couples.
[b] All concentrations are atomic percentages.
[c] Couple 9 was annealed for 25 h.

Table 2
Chemical analysis of U–Pu–Zr alloys

Nominal alloy	SEM/EDX on sample cross-section		Mass spectroscopy						
	Pu (at.%)	Zr (at.%)	Pu (at.%)	Zr (at.%)	Fe (wt ppm)	Ni (wt ppm)	Cu (wt ppm)	Si (wt ppm)	Y (wt ppm)
U	–	–	–	–	< 10	< 10	< 10	42 ± 11	< 20
U–20Zr	–	17.0 ± 1.5	–	21.5 ± 1.1	77 ± 8	< 10	< 10	147 ± 37	< 20
U–22Pu–3Zr	21.4 ± 0.6	1.5 ± 1.0	21.69 ± 0.11	3.83 ± 0.38	14 ± 1	< 10	< 10	119 ± 30	< 20
U–22Pu–20Zr	23.3 ± 0.3	19.7 ± 1.2	21.42 ± 0.11	22.9 ± 1.1	64 ± 6	< 10	< 10	–	< 20

bars were characterized by using the energy-dispersive X-ray (EDX) analysis capabilities of an ETEC Autoscan scanning electron microscope (SEM) housed in a plutonium glovebox. In addition, detailed chemical analyses were performed on sibling samples using mass spectroscopy. All Zr-bearing alloys contained inclusions that have been identified as impurity-stabilized zirconium [21,22]. For regions free of inclusions, SEM/EDX measurements were taken throughout the polished cross sections of the samples, using area scans to average the compositions in two-phase regions. Table 2 compares the SEM/EDX results with the mass spectroscopy results. Mass spectroscopy consistently reports higher Zr levels than SEM/EDX because it includes the zirconium-rich inclusions.

Couples 1 through 8 in Table 1 were assembled and annealed in two batches. The alloys were stacked into a test column that allowed four couples to be simultaneously annealed. All specimen preparation was performed remotely in plutonium gloveboxes. A diamond cut-off wheel was used to cut 3 mm long diffusion couple samples from the metal bars. Both ends of these cylindrical samples were ground and given a final polish using a 1 μm diamond paste. In addition, oxide films on the sides of the samples were removed with a diamond file. Immediately after polishing, a test column was made by stacking the samples into a Kovar alloy fixture [23]. A thermal expansion difference between the Kovar alloy (Fe–29 wt%Ni–17 wt%Co–0.3 wt%Mn–0.2 wt%Si) and the test column ensured axial compressive loading of the samples during annealing.

The annealed test columns were sliced with a diamond cut-off wheel, exposing a longitudinal section that was then ground and polished to a 1 μm finish for SEM examination. A Kevex 8000 EDX analysis system (Fisons Instruments) was used to analyze X-ray spectra collected at 30 keV with a 3 nA beam current. This energy allowed analysis of the U and Pu L-alpha peaks (13.61 keV and 14.28 keV, respectively), which do not suffer the severe overlap observed for the lower-energy M-lines. These lines are also well separated from the Zr K-alpha line (15.74 keV). The EDX data were converted to compositions by comparison with spectra of uranium dioxide, plutonium dioxide, and zirconium dioxide used as standards. The composition data were corrected for inter-element effects (ZAF correction factors) and were normalized to unity.

Composition profiles were generated by taking EDX spot measurements across each diffusion zone; the position of each spot was marked on SEM micrographs. To calibrate the magnification of the SEM, a 3 mm diameter disk punched from a 1000-mesh copper grid was attached to each mount with carbon paint. The grid spacings were compared with an objective micrometer under an oil-immersion microscope. Measurements confirmed that the grid spacings were 25.55 ± 0.27 μm, as expected for a 1000-mesh screen. In this way, an accurate magnification could be calculated for each SEM session to determine the distances between EDX measurement locations.

4. Results and discussion

4.1. Composition and interdiffusion flux profiles

The composition data for all couples generated by the SEM/EDX analyses can be plotted as functions of distance to yield concentration profiles. Interdiffusion data can be calculated from analytic curves fitted to the profiles.

The concentration and interdiffusion flux profiles for the nine couples are presented in Figs. 1–7. The positions of the marker planes and the Matano planes are identified on these profiles. Although inert markers were not specifically used in these couples, the location of the marker plane in each couple could be identified by a row of zirconium-rich inclusions on the original polished faces perpendicular to the diffusion direction.

All couples had large diffusion zones. The ternary couples, in particular, had zones greater than 1000 μm wide. In general, Zr had a smaller interdiffusion flux than the other components. For the couples with pure U, the interdiffusion fluxes in the γ phase were larger in magnitude than those within the β phase at 1023 K.

Two binary diffusion couples were included in this study. A U versus U–20Zr couple (couple 8) was annealed at 1023 K for 16.5 h, whereas a U versus U–27Pu couple

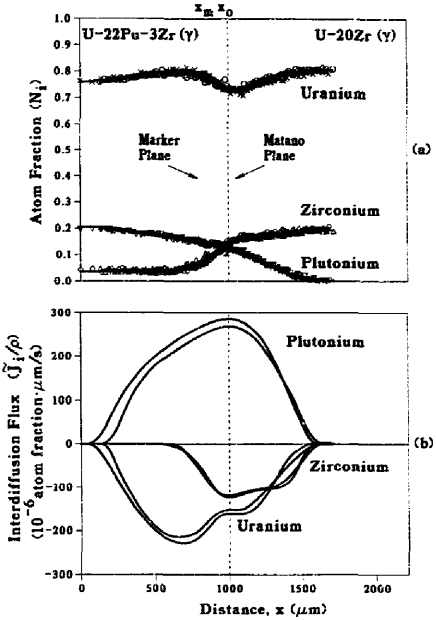

Fig. 1. Profiles of: (a) Concentration and (b) interdiffusion flux for the U–20Zr versus U–22Pu–3Zr couples annealed at 1023 K for 16.5 h – Couples 1 and 2.

(couple 9) was annealed at 1023 K for 25 h. As seen in the concentration profiles in Figs. 6 and 7, the diffusion zone width in couple 9 was greater than that in couple 8 by more than an order of magnitude. This difference in diffusion zone size cannot be explained solely by the difference in annealing time. Furthermore, the interdiffusion flux in the γ-U phase for couple 9 was approximately an order of magnitude greater than for couple 8. These observations indicate that the interdiffusivity in the U–Pu system is substantially greater than in the U–Zr system at this temperature.

4.2. Experimental diffusion paths

A diffusion path for a couple can be represented by plotting the sequence of compositions from the composition/distance profiles on an isothermal ternary phase diagram. This plot contains no spatial or kinetic information about the diffusion zone, but is useful as it provides a time-independent representation of the compositions and phases developed in the couple.

Fig. 8 presents the diffusion paths for seven of the nine experiments and includes the Matano and marker plane compositions. (Diffusion paths for couples 1 and 4, the replicates of couples 2 and 5, are not shown to reduce confusion among similar plots.) Notable in some of these diffusion paths are path segments of nearly constant Zr content near 20 at.% Pu. In these regions, U and Pu interdiffuse with little Zr migration. This observation is consistent with diffusion path predictions for a system with one component (in this case, Pu) that is significantly faster than the other two [24].

4.3. Experimental binary interdiffusion coefficients

4.3.1. U–Zr system

Couples 8 and 9 constitute two binary couples in this study. The U versus U–20Zr couple (couple 8) exhibits β and γ phase layers separated by a planar interface. The binary interdiffusion coefficient $\tilde{D}$ for couple 8 is plotted as a function of zirconium content in Fig. 9. Diffusion coefficients are only plotted over a limited composition range, since negligibly small concentration gradients near the ends of the diffusion zone and near the β/γ phase boundary lead to large errors in $\tilde{D}$. Also plotted are the average effective interdiffusion coefficients in the β-U and γ-U phases. These coefficients are listed in Table 3 along with values for the other diffusion couples.

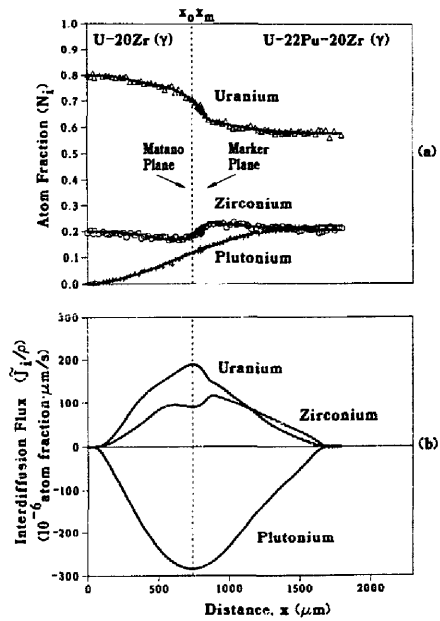

Fig. 2. Profiles of: (a) Concentration and (b) interdiffusion flux for the U–20Zr versus U–22Pu–20Zr couple annealed at 1023 K for 16.5 h – Couple 3.

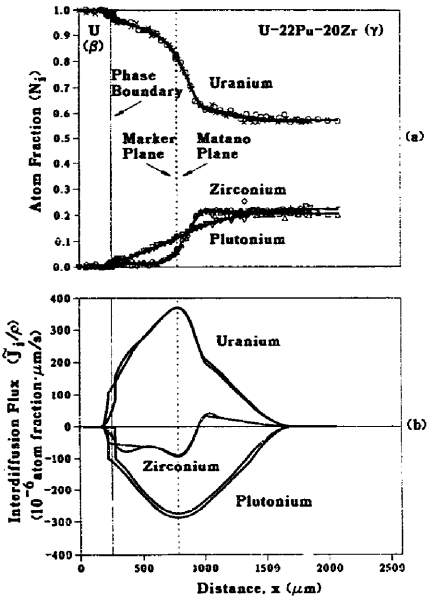

Fig. 3. Profiles of: (a) Concentration and (b) interdiffusion flux for the U versus U–22Pu–20Zr couples annealed at 1023 K for 16.5 h – Couples 4 and 5.

From Fig. 9, in the γ-U phase there is a continuous decrease in the composition-dependent interdiffusion coefficient with increases in zirconium concentration; the interdiffusivity decreases by an order of magnitude as the zirconium content increases from 4 at.% to 17 at.%. This observation can be related to the composition profile in Fig. 6. The Zr concentration gradient steepens going from the β/γ phase boundary to the 390 μm position, whereas the magnitude of the interdiffusion flux remains consistently greater than 30×10^{-6} atom fraction μm/s, thus requiring a substantial change in the interdiffusion coefficient in accordance with Eq. (2).

In 1959 Philibert and Adda reported data from uranium–zirconium chemical diffusion experiments performed between 863 K and 1223 K [3]. Their data have recently been re-analyzed to evaluate interdiffusion fluxes, composition-dependent diffusion coefficients, average effective diffusivities, and activation energies [25]. The re-analyzed concentration and interdiffusion flux profiles for their 89 h diffusion experiment at 1025 K is presented in Fig. 10. The concentration-dependent binary interdiffusion coefficient is plotted as a function of zirconium concentration in Fig. 11. The results are consistent with those from couple 8 in that a steepening of the Zr concentration gradient reflects an order of magnitude decrease in the interdiffusion coefficient, especially for zirconium concentrations greater than 15 at.%. An average effective interdiffusion coefficient calculated for Philibert and Adda's couple over the same composition range as the γ phase in couple 8 corresponds to 0.04×10^{-12} m^2/s, which compares well with the value of 0.03×10^{-12} m^2/s for couple 8 (Table 3).

4.3.2. U–Pu system

Binary γ-phase interdiffusion coefficients calculated from the U versus U–27Pu couple (couple 9) are shown in Fig. 12 as a function of plutonium concentration. (The diffusion depth in the β phase was too small for accurate diffusivity calculations.) In the γ-U phase, $\tilde{D}$ increases by a factor of two as plutonium concentration increases from 10% to 25%. This increase can be explained qualitatively by an intrinsic Pu diffusivity that is an order of magnitude greater than the U intrinsic diffusivity [20]. Since the marker plane could not be identified in this couple, no quantitative conclusions can be drawn on intrinsic diffusion of the components.

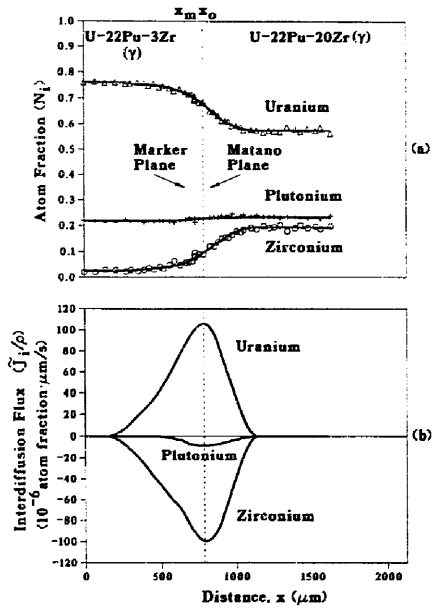

Fig. 4. Profiles of: (a) Concentration and (b) interdiffusion flux for the U–22Pu–3Zr versus U–22Pu–20Zr couple annealed at 1023 K for 16.5 h – Couple 6.

4.3.3. Zr–Pu system

Remy conducted binary diffusion couple experiments between pure Zr and Zr–Pu alloys with plutonium concentrations up to 70 at.% [4–6]. The interdiffusion coefficient data for the bcc phase at 1023 K reported in Ref. [6] are plotted in Fig. 13. The Zr–Pu interdiffusion coefficient increases with increasing Pu content (and, thus, decreases with increasing Zr content). This trend is consistent with the U–Pu and U–Zr binary couples, which exhibited, respectively, an increasing interdiffusion coefficient with increasing Pu levels (Fig. 12) and a decreasing interdiffusion coefficient with increasing Zr levels (Fig. 9). From these figures, the interdiffusion coefficient in the Zr–Pu system is approximately an order of magnitude less than that in the U–Pu system, but is generally greater than that for the U–Zr bcc phase.

4.4. Experimental ternary interdiffusion coefficients

4.4.1. $\tilde{D}_i^{eff}$ values

As listed in Table 3, average effective interdiffusion coefficients and effective penetration depth values for all nine couples have been calculated for the region to the left of the Matano plane, for the region to the right of the Matano plane, and for the entire γ-phase region. Values are not listed for regions over which the concentration change of the component is less than 2 at.%. Results from replicate couples 1 and 2 as well as from replicate couples 4 and 5 match within 20%. The γ-phase $\tilde{D}_i^{eff}$ values to the left and to the right of the Matano planes are shown schematically in Figs. 14–16 for Zr, U, and Pu, respectively.

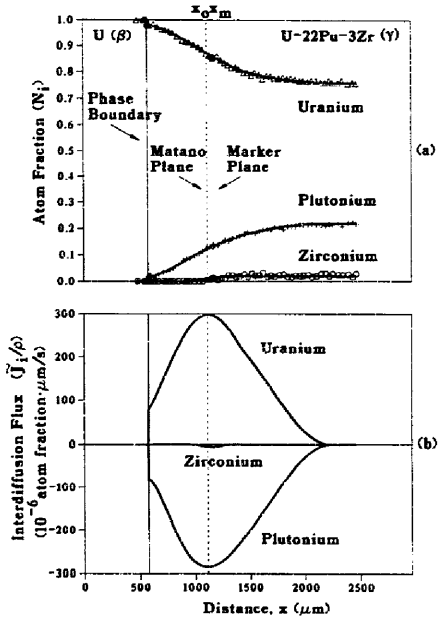

Fig. 5. Profiles of: (a) Concentration and (b) interdiffusion flux for the U versus U–22Pu–3Zr couple annealed at 1023 K for 16.5 h – Couple 7.

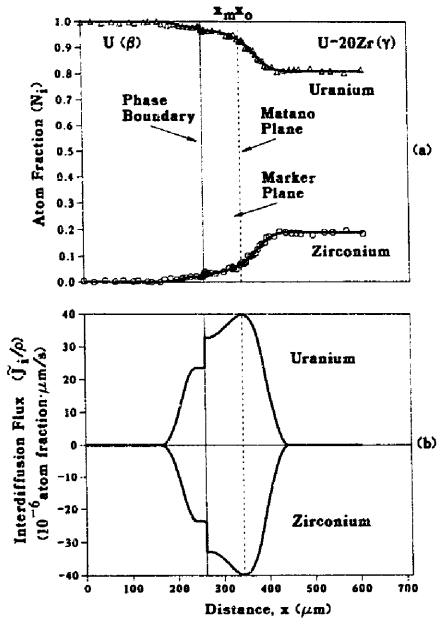

Fig. 6. Profiles of: (a) Concentration and (b) interdiffusion flux for the U versus U–20Zr couple annealed at 1023 K for 16.5 h – Couple 8.

A comparison of the γ-phase $\tilde{D}_i^{eff}$ values in Table 3 for couples 6 and 8 illustrates the effect of Pu on the interdiffusion coefficient. Both couples have Zr levels ranging up to 20 at.% and have constant Pu concentrations. Couple 8, a binary couple between U and U–20Zr alloys, has a γ-phase average effective interdiffusion coefficient of 0.03 $\times 10^{-12}$ m^2/s. In contrast, couple 6, which consisted of a U–22Pu–3Zr alloy annealed with a U–22Pu–20Zr alloy, produces an average effective diffusion coefficient of 0.27 $\times 10^{-12}$ m^2/s for zirconium and 0.25 $\times 10^{-12}$ m^2/s for uranium, approximately an order of magnitude greater than that for the binary couple. The addition of plutonium clearly increases the interdiffusion coefficients for the components.

In contrast, the addition of Zr decreases interdiffusivity

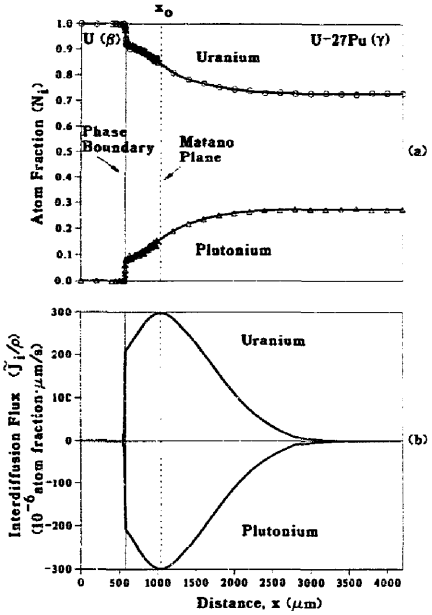

Fig. 7. Profiles of: (a) Concentration and (b) interdiffusion flux for the U versus U–27Pu couple annealed at 1023 K for 25 h – Couple 9. (Adapted from Ref. [20], with kind permission from Elsevier Science B.V., Amsterdam.)

in the γ phase. From Fig. 15, a comparison can be made of the $\tilde{D}_U^{eff}$ values in the constant-Zr couples 3, 7, and 9. At low plutonium levels, increasing the zirconium concentration from 0 to 20 at.% results in a decrease in $\tilde{D}_U^{eff}$ from

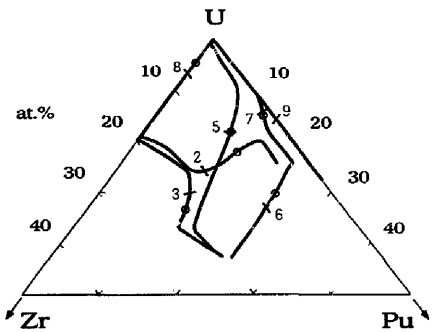

Fig. 8. Experimental diffusion paths at 1023 K with the compositions of the Matano (|) and Marker (○) planes identified. Couples 1 and 4 (not shown) are replicates of couples 2 and 5.

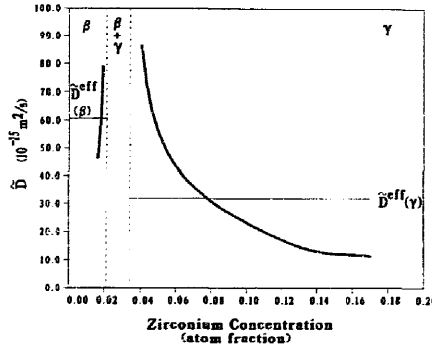

Fig. 9. Binary interdiffusion coefficient versus zirconium concentration for the U versus U–20Zr couple annealed at 1023 K for 16.5 h – Couple 8.

1.5×10^{-12} m²/s to 0.72×10^{-12} m²/s. At higher Pu contents, $\tilde{D}_U^{eff}$ decreases by a factor of three (from 2.2×10^{-12} m²/s to 0.59×10^{-12} m²/s) as Zr is increased to 20 at.%. From Fig. 16, the plutonium average effective interdiffusion coefficient $\tilde{D}_{Pu}^{eff}$ is less dependent on Zr

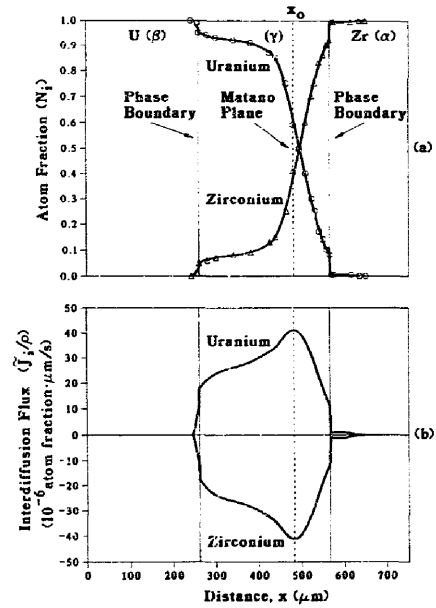

Fig. 10. Profiles of: (a) Concentration and (b) interdiffusion flux for the U versus Zr couples annealed at 1025 K for 89 h [3].

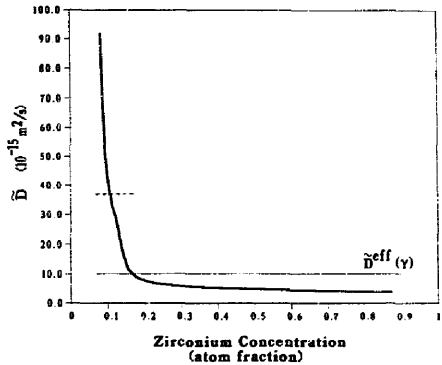

Fig. 11. Binary interdiffusion coefficient versus zirconium concentration in the bcc γ phase for the Ref. [3] U versus Zr diffusion couple annealed at 1025 K for 89 h. (The dashed line represents the average interdiffusion coefficient over the same composition range as in the couple 8 γ phase (5–20 at.%).)

content, though it does decrease by a factor of 1.6 over the same Zr range. Even small additions of Zr reduce the $\tilde{D}^{eff}_{U}$ and $\tilde{D}^{eff}_{Pu}$ interdiffusion coefficients. The zirconium concentration in couple 7 is at most 3 at.%, yet the average effective interdiffusion coefficients for this couple are consistently 30% less than those for couple 9, which contains no zirconium. These constant-Zr experiments show that the side of the couple with the higher Pu level has higher average effective interdiffusion coefficients. An exception is couple 3, which exhibits a 22% greater $\tilde{D}^{eff}_{U}$ value on the low-Pu side (0.72×10^{-12} m^2/s) than on the high-Pu side (0.59×10^{-12} m^2/s).

4.4.2. $\tilde{D}^{3}_{ij}$ matrix

The $\tilde{D}^{3}_{ij}$ matrix can be determined at the common composition of two diffusion couples with intersecting diffusion paths. Some of the $\tilde{D}^{3}_{ij}$ elements can also be calculated from individual couples at compositions with near-zero concentration gradients for one of the components in the diffusion zone. Table 4 lists the elements of

Table 3
Average effective interdiffusion coefficients

Couple	Element	x_o (μm)	Matano plane concentration (atom fraction)	$\tilde{D}^{eff}_{i}$ (γ) (10^{-12} m^2/s)	$\bar{x}_\gamma$ (μm)	Toward binary or pure U side [a]		Toward ternary side	
						$\tilde{D}^{eff}_{left}$ (10^{-12} m^2/s)	$\bar{x}_l$ (μm)	$\tilde{D}^{eff}_{right}$ (10^{-12} m^2/s)	$\bar{x}_r$ (μm)
1	Zr	990	0.15	0.44	230	0.88	323	0.21	160
	U	998	0.73	–	–	0.83	315	–	–
	Pu	999	0.12	1.4	402	0.86	319	2.1	499
2	Zr	988	0.14	0.48	238	0.96	337	0.23	164
	U	1010	0.74	–	–	0.74	296	–	–
	Pu	1002	0.12	1.2	381	0.86	319	1.7	453
3	Zr	741	0.18	–	–	–	–	–	–
	U	742	0.70	0.65	278	0.72	293	0.59	265
	Pu	736	0.12	1.2	373	1.0	345	1.4	402
4	Zr	782	0.07	0.18	146	0.70	289	–	–
	U	783	0.82	0.67	283	0.97	340	0.50	244
	Pu	782	0.11	1.2	374	1.1	366	1.2	382
5	Zr	783	0.06	0.18	147	0.67	283	–	–
	U	782	0.82	0.68	284	0.93	333	0.52	249
	Pu	784	0.12	1.3	388	1.2	384	1.3	391
6	Zr	793	0.10	0.27	180	0.38	212	0.19	150
	U	782	0.68	0.25	174	0.35	205	0.18	145
	Pu	775	0.22	–	–	–	–	–	–
7	Zr	1153	0.01	0.05	76	–	–	–	–
	U	1116	0.87	1.2	377	1.0	348	1.4	404
	Pu	1107	0.12	1.3	394	1.0	349	1.6	437
8 [b]	Zr	343	0.07	0.03	61	0.08	97	0.02	45
	U	343	0.93	0.03	61	0.08	97	0.02	45
9	U	1038	0.84	1.9	586	1.5	374	2.2	630
	Pu	1038	0.16	1.9	586	1.5	374	2.2	630

[a] For γ phase only.
[b] The average effective diffusion coefficient in the β phase for both Zr and U is 0.6×10^{-12} m^2/s with a penetration depth of 86 μm.

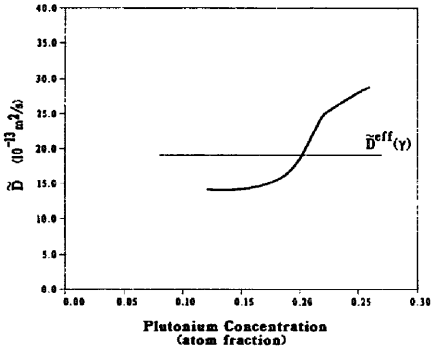

Fig. 12. Binary interdiffusion coefficient versus plutonium concentration for the U versus U–27Pu couple annealed at 1023 K for 25 h – couple 9. (Adapted from Ref. [20], with kind permission from Elsevier Science B.V., Amsterdam.)

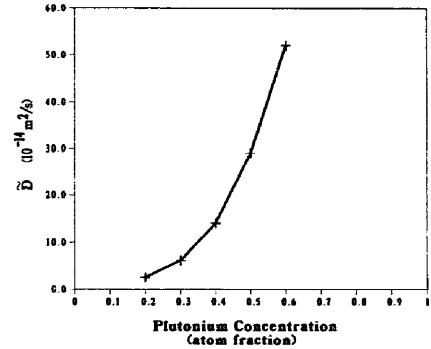

Fig. 13. Binary interdiffusion coefficient versus plutonium concentration in the bcc γ phase for the Ref. [6] Zr versus Zr–Pu diffusion couples annealed at 1023 K.

the [$\tilde{\mathbf{D}}$] matrix calculated at diffusion path intersections along with $\tilde{D}^3_{ij}$ elements determined at concentration maxima and minima. Results from replicate couples show good reproducibility, though there are greater variations in the cross coefficients ($i \neq j$) than in the main coefficients.

As listed in Table 4, at the common composition of couples 1 and 4 a $\tilde{D}^U_{ZrZr}$ coefficient of 0.16×10^{-12} m^2/s was calculated. This main coefficient, which gives the dependence of the zirconium interdiffusion flux on the Zr concentration gradient, is approximately 50% smaller than the magnitude of the negative cross-diffusion coefficient $\tilde{D}^U_{ZrPu}$. Hence, the Zr interdiffusion flux is affected less by the Zr concentration gradient than by the Pu concentration gradient. The negative $\tilde{D}^U_{ZrPu}$ coefficient indicates that Zr interdiffuses up a positive Pu concentration gradient toward regions of higher Pu contents. The main coefficient for plutonium, $\tilde{D}^U_{PuPu}$, is 1.7×10^{-12} m^2/s an order of magnitude greater than that for zirconium, $\tilde{D}^U_{ZrZr}$. For plutonium the magnitude of the cross coefficient $\tilde{D}^U_{PuZr}$ is more than an order of magnitude smaller than that of the main coefficient $\tilde{D}^U_{PuPu}$. Thus, Pu interdiffusion is affected strongly by its own concentration gradient, but is relatively uninfluenced by the Zr concentration gradient.

The diffusion paths in Fig. 8 highlight this distinction between Pu and Zr diffusion behavior. In couple 6 the Pu concentration remains approximately constant, whereas the Zr level in couple 3 varies widely. This difference is attributable to the cross-diffusivity terms for the two elements; unlike the Pu flux, the Zr flux is strongly driven by concentration gradients of the other components.

For couples 1 and 2, the uranium concentration profiles include a maximum and a minimum where $\partial C_U/\partial x = 0$. At these compositions, values for $\tilde{D}^{Pu}_{ZrZr}$ and $\tilde{D}^{Pu}_{UZr}$ can be determined on the basis of Eqs. (3) and (4) and are listed in Table 4. In addition, the $\tilde{D}^U_{ij}$ values calculated for the intersecting diffusion paths can be converted to $\tilde{D}^{Pu}_{ij}$ values from Eqs. (5)–(8). $\tilde{D}^{Pu}_{ZrZr}$ increases by more than a factor of three as the zirconium concentration increases from 4 at.% to 16 at.%. Conversely, $\tilde{D}^{Pu}_{UZr}$ decreases by at least a factor of two over the same range of Zr content.

Table 4
Ternary interdiffusion coefficients

Location	Composition (at.%)			Interdiffusion coefficients (10^{-12} m^2/s)					
	Zr	U	Pu	$\tilde{D}^U_{ZrZr}$	$\tilde{D}^U_{ZrPu}$	$\tilde{D}^U_{PuZr}$	$\tilde{D}^U_{PuPu}$	$\tilde{D}^{Pu}_{ZrZr}$	$\tilde{D}^{Pu}_{UZr}$
Intersection of couples 1 and 4	12	75	13	0.16	−0.33	−0.10	1.7	0.49 [a]	1.3 [b]
Intersection of couples 2 and 5	12	75	13	0.16	−0.29	−0.04	1.5	0.45 [a]	1.1 [b]
Zr minimum in couple 3	17	74	9	–	−0.45	–	1.3		
Zr maximum in couple 3	23	62	15	–	−0.62	–	1.4		
U maximum in couple 1	4	80	16					0.20	1.7
U maximum in couple 2	4	80	16					0.06	3.1
U minimum in couple 1	16	73	11					0.63	0.84
U minimum in couple 2	15	74	11					0.72	0.94

[a] Calculated from Eq. (5).
[b] Calculated from Eq. (7).

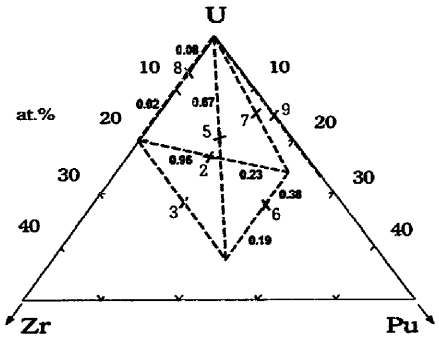

Fig. 14. Average effective interdiffusion coefficients (10^{-12} m^2/s) for zirconium in the bcc phase at 1023 K.

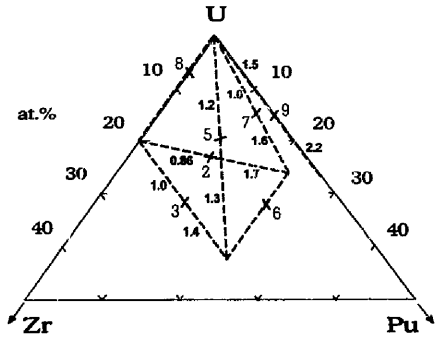

Fig. 16. Average effective interdiffusion coefficients (10^{-12} m^2/s) for plutonium in the bcc phase at 1023 K.

Several diffusion couples developed regions with negligibly small concentration gradients for one of the components. Couple 6, for instance, consisted of a U–22Pu–20Zr alloy bonded with a U–22Pu–3Zr alloy. Virtually no plutonium migration occurred in this couple, such that most interdiffusion occurred between U and Zr, as can be seen from the concentration profiles in Fig. 4. Therefore, $\tilde{D}^{U}_{ZrZr}$ can be calculated along portions of the diffusion zone with small Pu concentration gradients and can be compared with the binary U–Zr interdiffusion coefficients for couple 8. These results are presented in Fig. 17 as a function of zirconium concentration. In both couples 6 and 8, the interdiffusion coefficient decreases as zirconium content increases. Nevertheless, the presence of 22% Pu in couple 6 has increased the interdiffusion coefficient by an order of magnitude above the U–Zr binary diffusivity. A similar increase in the average effective interdiffusion coefficients for zirconium is observed in Fig. 14. Also included in Fig. 17 are the $\tilde{D}^{U}_{ZrZr}$ values calculated at the common compositions between couples 1 and 4 and between couples 2 and 5 at approximately 13 at.% Pu. For this intermediate concentration of plutonium, the value of $\tilde{D}^{U}_{ZrZr}$ lies between those calculated for couples 6 and 8. This observation further supports the conclusion that the zirconium interdiffusion coefficient increases with increasing Pu content at 1023 K.

Several ternary diffusion couples developed regions with near-zero Zr concentration gradients. In these regions, the main plutonium interdiffusion coefficient $\tilde{D}^{U}_{PuPu}$ can be determined. These values are plotted in Fig. 18 as a function of plutonium concentration and are compared with the couple 9 binary U–Pu interdiffusion coefficients and with the $\tilde{D}^{U}_{PuPu}$ values tabulated in Table 4. The $\tilde{D}^{U}_{PuPu}$

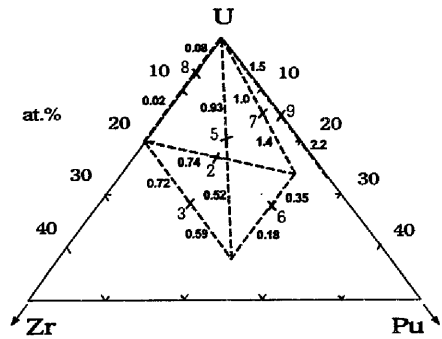

Fig. 15. Average effective interdiffusion coefficients (10^{-12} m^2/s) for uranium in the bcc phase at 1023 K.

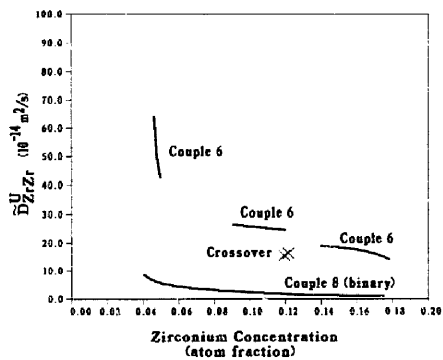

Fig. 17. Main zirconium interdiffusion coefficient versus zirconium concentration. (The crossover values are those calculated for the common compositions between couples 1 and 4 and between couples 2 and 5.)

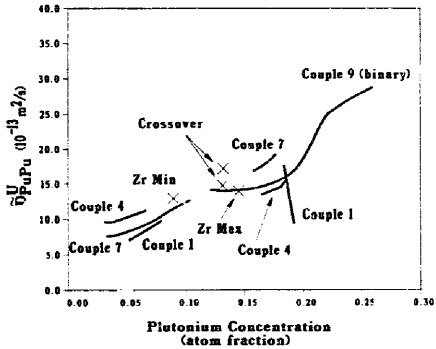

Fig. 18. Main plutonium interdiffusion coefficient versus plutonium concentration.

values increase threefold as the Pu content is raised to 25%; the values are affected little by the Zr content, which ranges from 0 to 23 at.%. This conclusion, that the main coefficient for Pu is essentially independent of Zr or U concentration, is consistent with the composition dependencies noted for the plutonium average effective interdiffusion coefficients in Fig. 16.

Ishida et al. [11] calculated $\tilde{D}_{ij}^{Pu}$ coefficients for a U–16.3Pu–22.5Zr alloy based on an ideal ternary solid solution model and published uranium self-diffusion coefficients. A tracer diffusion coefficient for zirconium was estimated to be the uranium self-diffusion coefficient times the ratio of the zirconium and uranium intrinsic diffusion coefficients from published binary studies. The plutonium tracer diffusion coefficient was arbitrarily assumed to be 1.2 times the uranium self-diffusion coefficient. From Eqs. (5)–(8), their ternary interdiffusion coefficients can be translated to the uranium solvent system, yielding for 1023 K:

$$\tilde{D}^{U}_{ZrZr} = 0.15 \times 10^{-12}\ m^2/s,$$

$$\tilde{D}^{U}_{ZrPu} = -0.005 \times 10^{-12}\ m^2/s,$$

$$\tilde{D}^{U}_{PuZr} = 0.02 \times 10^{-12}\ m^2/s,$$

$$\tilde{D}^{U}_{PuPu} = 0.27 \times 10^{-12}\ m^2/s.$$

Compared with the experimental coefficients listed in Table 4, Ishida's $\tilde{D}^{U}_{PuPu}$ value is lower by a factor of six, and $\tilde{D}^{U}_{ZrPu}$ by a factor of sixty. These discrepancies suggest that Ishida's tracer diffusivity estimates are inaccurate or that the ideal solution model is inappropriate for the U–Pu–Zr system at this temperature.

4.5. Experimental intrinsic diffusion coefficients

For multi-component systems, Eq. (16) defines a matrix of intrinsic diffusion coefficients, **[D]**, as a proportionality between the intrinsic fluxes and the concentration gradients. In a ternary system, two diffusion experiments are needed to determine the six independent D_{ij}^{3} values. Since the D_{ij}^{3} elements are typically dependent on composition, the two experiments must have marker planes with identical compositions. The calculated **[D]** matrix is then only applicable to this composition.

Couples 1 and 2 have diffusion paths that cross the paths of couples 4 and 5, but their marker plane compositions are different. Couple 1 has a marker plane composition of 78U–14Pu–8Zr, whereas the marker plane composition of couple 4 is 82U–12Pu–6Zr. If the intrinsic diffusivity is presumed to be constant over this small composition range, then the D_{ij}^{3} elements can be calculated from the couple 1/couple 4 and couple 2/couple 5 combinations. These data are reported in Table 5.

Table 5
Intrinsic diffusion coefficients

Diffusion couple	Marker plane concentration (at.%)			Intrinsic diffusion coefficients (10^{-12} m^2/s)						Binary intrinsic diffusion coefficients (10^{-12} m^2/s)		
	Zr	U	Pu	D^{U}_{ZrZr}	D^{U}_{ZrPu}	D^{U}_{UZr}	D^{U}_{UPu}	D^{U}_{PuZr}	D^{U}_{PuPu}	D_{Zr}	D_{U}	D_{Pu}
Couple 1	8	78	14	0.07	0.25	−1.8	2.8	−0.55	2.7			
Couple 4	6	82	12									
Couple 2	8	78	14	0.05	0.29	−1.6	2.4	−0.40	2.3			
Couple 5	6	82	12									
U–Zr binary couple 8	5	95	–							0.04	0.25	
Zr–Pu binary (Remy [5])	80	–	20							0.019		0.025
	62	–	38							0.044		0.17
	43.5	–	56.5							0.21		0.79

The main coefficient for plutonium, D^{U}_{PuPu}, is forty times greater than the main coefficient for zirconium, D^{U}_{ZrZr}. The intrinsic Zr flux is affected more by the cross coefficient D^{U}_{ZrPu} than by the smaller D^{U}_{ZrZr} term.

In a binary system, the two independent intrinsic diffusion coefficients can be solved directly from Eq. (17) based on a single diffusion couple experiment. Table 5 includes binary intrinsic diffusion coefficients for the U–Zr binary couple (couple 8) and values reported by Remy [5] for the Zr–Pu system. For a marker composition of U–5Zr, the binary zirconium intrinsic diffusion coefficient is approximately the same as the ternary $\tilde{D}^{U}_{ZrZr}$ value calculated for the couple 2 and couple 5 marker planes. From couple 8, D_U is more than six times greater than D_{Zr}.

From Zr–Pu binary diffusion experiments at 750°C, Remy [5] found that Pu has a greater intrinsic diffusion coefficient than Zr (Table 5). The intrinsic diffusion coefficients for both elements increase with increasing Pu content.

5. Summary

Isothermal diffusion couple experiments with body-centered cubic U–Pu–Zr alloys were performed at 1023 K. The compositions of the U–Pu–Zr alloys used in these experiments covered the uranium-rich corner of the ternary phase diagram with plutonium concentrations up to 27 at.% and zirconium concentrations up to 20 at.%. Ternary interdiffusion coefficients were calculated at the common composition between two couples with intersecting diffusion paths. The cross coefficient for zirconium, $\tilde{D}^{U}_{ZrPu}$, is calculated to be negative and twice the magnitude of the main coefficient, $\tilde{D}^{U}_{ZrZr}$. The negative value of $\tilde{D}^{U}_{ZrPu}$ indicates that zirconium interdiffuses up a plutonium concentration gradient in the absence of other driving forces. In contrast, $\tilde{D}^{U}_{PuZr}$ is negligible compared with $\tilde{D}^{U}_{PuPu}$, which is an order of magnitude greater than $\tilde{D}^{U}_{ZrZr}$. That is, zirconium concentration gradients have little effect on the Pu interdiffusion flux. $\tilde{D}^{U}_{PuPu}$ increases by a factor of three as the Pu concentration is increased from 4 at.% to 25 at.%, but is essentially independent of the concentration of uranium and zirconium. The Pu average effective interdiffusion coefficient also increases with increasing Pu content. In general, the uranium and zirconium average effective interdiffusion coefficients decrease with an increasing Zr concentration and increase with an increasing Pu concentration.

Intrinsic diffusion coefficients were determined for a binary U–5Zr composition and for a ternary composition of approximately U–13Pu–7Zr. For the binary composition, D_U is approximately six times greater than D_{Zr}. For the ternary composition, the main intrinsic diffusion coefficient for plutonium, D^{U}_{PuPu}, is forty times greater than the main coefficient for zirconium, D^{U}_{ZrZr}.

Acknowledgements

The authors thank R.A. Blomquist, A.G. Hins, D.D. Keiser Jr., L. Leibowitz, J.E. Sanecki, and P.C. Tortorici for assistance with the experiments and analyses. This work was supported by the US Department of Energy, Reactor Systems, Development and Technology, under Contract No. W-31-109-ENG-38.

References

[1] B.R. Seidel, L.C. Walters and Y.I. Chang, J. Met. 39 (4) (1987) 10.
[2] T. Hiraoka, K. Sako, H. Takano, T. Ishii and M. Sato, Nucl. Technol. 93 (1991) 305.
[3] J. Philibert and Y. Adda, Colloque sur la Diffusion à L'état Solide (North-Holland, Amsterdam, 1959) p. 163.
[4] C. Remy, Diffusion et Effet Kirkendall Dans le Système Plutonium–Zirconium, Commissariat a l'Energie Atomique Rapport CEA-R-3573 (Oct. 1968).
[5] C. Remy, M. Dupuy and M.D. Calais, in: Quantitative Relation Between Properties and Microstructure, ed.s D.G. Brandon and A. Rosen (Israel Universities Press, Jerusalem, 1969) p. 435.
[6] C. Remy, M. Dupuy and D. Calais, J. Nucl. Mater. 34 (1970) 46.
[7] P.K. Talley, A.D. Pelton and L. Leibowitz, Thermodynamic Modeling of Phase Equilibria in the Pu–U–Zr System, to be published.
[8] S.J. Rothman, L.T. Lloyd and A.L. Harkness, Trans. AIME 218 (1960) 605.
[9] M. Dupuy and D. Calais, Trans. AIME 242 (1968) 1679.
[10] J.I. Federer and T.S. Lundy, Trans. AIME 227 (1963) 592.
[11] M. Ishida, T. Ogata and M. Kinoshita, Nucl. Technol. 104 (1993) 37.
[12] M.A. Dayananda and C.W. Kim, Metall. Trans. A10 (1979) 1333.
[13] L. Onsager, Phys. Rev. 37 (1931) 405.
[14] L. Onsager, Phys. Rev. 38 (1931) 2265.
[15] T.O. Ziebold and R.E. Ogilvie, Trans. AIME 239 (1967) 942.
[16] M.A. Dayananda and D.A. Behnke, Scr. Metall. Mater. 25 (1991) 2187.
[17] T. Heumann, Z. Phys. Chem. 201 (1952) 168.
[18] A.G. Guy and J. Philibert, Z. Metallkd. 56 (1965) 841.
[19] M.A. Dayananda, Defect Diffus. Forum 83 (1992) 73.
[20] M.C. Petri, A.G. Hins, J.E. Sanecki and M.A. Dayananda, J. Nucl. Mater. 211 (1994) 1.
[21] D.R. O'Boyle and A.E. Dwight in: Plutonium 1970 and Other Actinides, ed. W.N. Miner (Metallurgical Society of the AIME, New York, 1970) p. 720.
[22] S.M. McDeavitt and A.A. Solomon, in: Advances in Powder Metallurgy and Particulate Materials 1992, eds. J.M. Capus and R.M. German, Vol. 6 (Metal Powder Industries Federation, Princeton, NJ, 1992) p. 109.
[23] M.C. Petri, PhD thesis, Purdue University (May 1995).
[24] R.T. DeHoff, K.J. Anusavice and C.C. Wan, Metall. Trans. 5 (1974) 1113.
[25] G.L. Hofman, S.L. Hayes and M.C. Petri, J. Nucl. Mater. 227 (1996) 277.